IMA Journal of Applied Mathematics (2024) **89**, 725–744
https://doi.org/10.1093/imamat/hxae028
Advance Access publication on 18 October 2024

Pendent steady rivulets and droplets: from lubrication to bifurcation

Michael Grinfeld and David Pritchard*
Department of Mathematics and Statistics, University of Strathclyde, 26 Richmond Street, Glasgow G1 1XH, Scotland, UK
*Corresponding author: david.pritchard@strath.ac.uk

[Received on 21 April 2023; revised on 3 September 2024; accepted on 9 October 2024]

We consider the shape of the free surface of steady pendent rivulets (or equivalently, two-dimensional droplets) beneath a planar substrate. We formulate the governing equations in terms of two closely related dynamical systems and use classical phase-plane techniques, in particular time maps, to analyse the bifurcation structure of the problem. Our results explain why lubrication theory is unable to capture this bifurcation structure for pendent rivulets, although it is successful in the related problem of sessile rivulets.

Keywords: rivulets; surface tension; bifurcation analysis; time maps.

1. Introduction

Rivulet flow on or beneath an inclined substrate has been the subject of many mathematical modelling studies, motivated by industrial and scientific applications, since the seminal work of Duffy & Moffatt (1995). The physics of such flows is well understood, and implicit exact solutions to the full non-linear problem have been presented (e.g. Perazzo & Gratton, 2004; Tanasijczuk *et al.*, 2010; Sokurov, 2020). There is, however, a problem that is most clearly seen in the case of a *pendent, perfectly wetting* rivulet: the classical lubrication approach (e.g. Duffy & Moffatt, 1995; Wilson & Duffy, 2005), which is frequently used in parametric studies and extensions of the basic rivulet problem (e.g. Sullivan *et al.*, 2008; Paterson *et al.*, 2013, 2014), yields non-unique solutions that are defined only for particular rivulet widths.

It is generally believed (see e.g. Snoeijer, 2006) that in many contexts the lubrication approach yields valid qualitative predictions even when it is not quantitatively accurate. In the case of pendent, perfectly wetting rivulets, however, this approach clearly yields *qualitatively* incorrect results. Thus the main purpose of this study is to elucidate the relationship between the lubrication approximation solutions and the bifurcation structure of the full non-linear boundary-value problem that describes the shape of a rivulet, focusing on perfectly wetting pendent rivulets. The approach that we take permits a rigorous analysis using the method of time maps (Schaaf, 1991), and extends previous treatments of the problem that mainly relied on the computation of elliptic integrals.

We confine ourselves to investigating the cross-sectional profile of uniform steady rivulets. The flux of fluid along the rivulet can therefore be ignored, and our results may also be interpreted as the profiles of static two-dimensional drops (fluid ridges) attached to a horizontal substrate. The problem of characterizing drop profiles was first considered by Neumann (1894), and subsequently developed by many authors (e.g. Pitts, 1973; Majumdar & Michael, 1976; Sumesh & Govindarajan, 2010; Liu *et al.*, 2014; Roman *et al.*, 2020). Two physically important quantities that characterize such a profile are its width and its total area; since solutions are symmetrical about the centreline, it will be convenient to consider the half-width and the half-area instead. We note that the width of a rivulet on an inclined plane

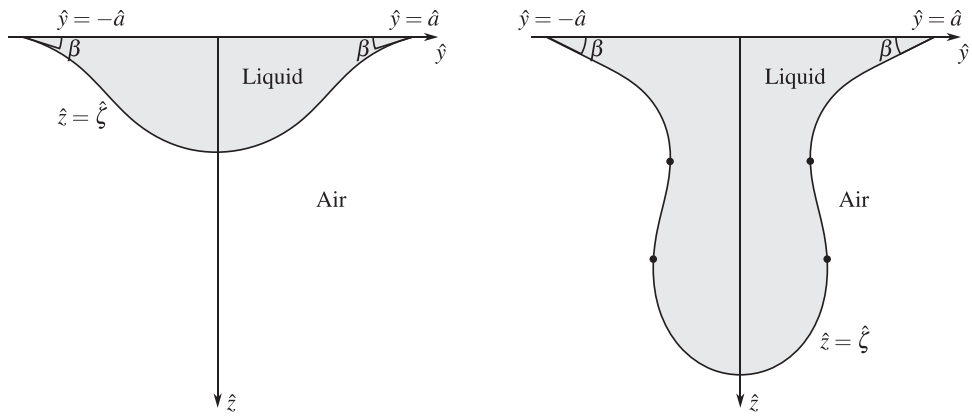

FIG. 1. Schematic showing the profiles of pendent rivulets with and without an overhang. The black dots represent 'critical points' at which the free surface is vertical.

can be controlled by chemically modifying the substrate and therefore it is experimentally feasible to take the width as a bifurcation parameter, as we do below.

We consider only the existence of solutions. An unequivocal assignment of stability to different solution branches is still a matter of debate; the reader is referred to Pitts (1973); Majumdar & Michael (1976); Sumesh & Govindarajan (2010).

The structure of the paper is as follows. In Section 2, we discuss the governing equations and the alternative approach that takes the arclength along the free surface as the independent variable. In Section 3, we formulate the governing equations in terms of two related phase planes, and describe the construction of solutions for perfectly wetting pendent rivulets in terms of orbits in these phase planes, including the crucial time map (Section 3.2). In Section 4, we carry out a thorough bifurcation analysis of these solutions. In Section 5, we discuss extensions to imperfectly wetting rivulets. Finally, in Section 6 we collect our conclusions.

2. Governing equations

We consider uniform steady pendent rivulets below a planar substrate that is inclined at an angle α to the horizontal; as shown in Fig. 1, $\hat{z}$ is the coordinate perpendicular to the plane and increasing *downwards*, and $\hat{y}$ is a horizontal coordinate parallel to the plane.

The key physical assumption (the Laplace–Young equation) is the boundary condition at a liquid–air interface

$$\hat{P} = \hat{\gamma}\hat{C}, \tag{2.1}$$

where $\hat{P}$ is the excess pressure in the liquid relative to that in the air, $\hat{\gamma}$ is the coefficient of surface tension and $\hat{C}$ is the (signed) curvature of the interface, defined such that if the liquid is on the same side as the centre of curvature then $\hat{C} > 0$ (See e.g. Batchelor (1967), pp. 61–64).

If we can write the free surface locally as $\hat{z} = \hat{\zeta}(\hat{y})$ for some function $\hat{\zeta}(\hat{y})$ then we may evaluate $\hat{C}$ as

$$\hat{C} = \frac{\pm\hat{\zeta}''}{[1 + (\hat{\zeta}')^2]^{3/2}}, \tag{2.2}$$

where the positive sign is taken if the liquid occupies $\hat{z} > \hat{\zeta}$, and the negative sign is taken if the liquid occupies $\hat{z} < \hat{\zeta}$.

REMARK 1. This sign change is omitted from some presentations, leading to possible confusion. For example, the right-hand part of fig. 3 in Tanasijczuk *et al.* (2010) is not physically possible in the orientation shown.

We will be concerned with points $\hat{y} = \hat{y}_0$ on the free surface such that $|\hat{\zeta}'| \to \infty$ as $\hat{y} \to \hat{y}_0$, i.e. where the free surface is vertical. At such points the pressure, and thus from (2.1) the signed curvature $\hat{C}$, must be continuous. Below, we will call such points 'critical points'.

Suppose that for $\hat{y} < \hat{y}_0$ there are two interfaces $\hat{z} = \hat{\zeta}_1(\hat{y})$ and $\hat{z} = \hat{\zeta}_2(\hat{y}) > \hat{\zeta}_1(\hat{y})$, with liquid occupying $\hat{z} < \hat{\zeta}_1$ and $\hat{z} > \hat{\zeta}_2$, and suppose that these interfaces meet at $\hat{y} = \hat{y}_0$ (so $\hat{y}_0$ marks the point at which the free surface curves back and starts to overhang itself). From the discussion above, the appropriate conditions at the critical point $\hat{y}_0$ are thus

$$\begin{cases} \hat{\zeta}_1(\hat{y}_0) = \hat{\zeta}_2(\hat{y}_0), \\ \displaystyle\lim_{\hat{y}\to\hat{y}_0} \frac{-\hat{\zeta}_1''}{[1+(\hat{\zeta}_1')^2]^{3/2}} = \lim_{\hat{y}\to\hat{y}_0} \frac{+\hat{\zeta}_2''}{[1+(\hat{\zeta}_2')^2]^{3/2}}, \end{cases} \tag{2.3}$$

where the appropriate one-sided limit is assumed. It is simple to see that conditions (2.3) also apply if the liquid occupies $\hat{\zeta}_1 < \hat{z} < \hat{\zeta}_2$, or if the interfaces exist for $\hat{y} > \hat{y}_0$.

Within a uniform steady rivulet the pressure is hydrostatic and

$$\hat{P}(\hat{y}, \hat{z}) = \hat{\gamma}\hat{C} + \hat{\rho}\hat{g}\cos(\alpha)(\hat{z} - \hat{\zeta}(\hat{y})), \tag{2.4}$$

where $\hat{\rho}$ is the density of the liquid and $\hat{g}$ is the acceleration due to gravity, and where we evaluate $\hat{C}$ on the interface $\hat{z} = \hat{\zeta}$. (If the point $(\hat{y}, \hat{z})$ in the fluid lies between two interfaces, $\hat{\zeta}_1 < \hat{z} < \hat{\zeta}_2$, then we may take either $\hat{\zeta} = \hat{\zeta}_1$ or $\hat{\zeta} = \hat{\zeta}_2$ in (2.4)).

The hydrostatic condition $\partial\hat{P}/\partial\hat{y} = 0$ therefore becomes

$$\hat{\gamma}\frac{\mathrm{d}\hat{C}}{\mathrm{d}\hat{y}} - \hat{\rho}\hat{g}\cos(\alpha)\frac{\mathrm{d}\hat{\zeta}}{\mathrm{d}\hat{y}} = 0, \tag{2.5}$$

or on any given portion of the free surface,

$$\pm\hat{k}\hat{\zeta}' = \left[\frac{\hat{\zeta}''}{[1+(\hat{\zeta}')^2]^{3/2}}\right]', \tag{2.6}$$

where the positive sign is taken for sections of the free surface on which liquid lies below air, and the negative sign for sections on which liquid lies above air, and where the parameter $\hat{k}$ is given by

$$\hat{k} = \frac{\hat{\rho}\hat{g}}{\hat{\gamma}}\cos(\alpha) > 0. \tag{2.7}$$

Equation (2.6) is to be solved subject to suitable boundary conditions at the contact lines $\hat{y} = \pm\hat{a}$,

$$\hat{\zeta}(\pm\hat{a}) = 0 \qquad \text{and} \qquad \hat{\zeta}'(\pm\hat{a}) = \mp\tan(\beta), \tag{2.8}$$

where $\beta \geq 0$ is the contact angle and $\hat{a}$ is the half-width of the rivulet.

We may scale out $\hat{k}$ by defining

$$y = \sqrt{\hat{k}}\hat{y}, \qquad \zeta(y) = \sqrt{\hat{k}}\hat{\zeta}(\hat{y}), \qquad a = \sqrt{\hat{k}}\hat{a}, \tag{2.9}$$

to obtain the dimensionless system

$$k\zeta' = \left[\frac{\zeta''}{[1 + (\zeta')^2]^{3/2}}\right]' \tag{2.10}$$

subject to

$$\zeta(\pm a) = 0 \qquad \text{and} \qquad \zeta'(\pm a) = \mp\tan(\beta). \tag{2.11}$$

The parameter k takes only two values: $k = +1$ corresponds to a section of the interface with liquid below air, while $k = -1$ corresponds to a section of the interface with liquid above air.

Unless otherwise stated, we consider the case of a perfectly wetting fluid, for which the contact angle $\beta = 0$ and (2.11) becomes

$$\zeta(\pm a) = 0 \qquad \text{and} \qquad \zeta'(\pm a) = 0. \tag{2.12}$$

2.1 *Lubrication approximation*

The lubrication approximation, as applied in this context by Duffy and co-workers (e.g. Duffy & Moffatt, 1995; Wilson & Duffy, 2005; Sullivan *et al.*, 2008; Paterson *et al.*, 2013, 2014), corresponds to the limit of small free-surface gradients, $|\zeta'| \ll 1$. (We note that Snoeijer (2006) has presented a generalized lubrication approximation, valid for small capillary numbers but arbitrary surface slopes, which has the same structure as a classical lubrication approximation but preserves the full non-linear curvature term).

In the regime $|\zeta'| \ll 1$, the system (2.10) and (2.12) becomes

$$k\zeta' = \zeta''', \qquad \zeta(\pm a) = 0, \qquad \zeta'(\pm a) = 0. \tag{2.13}$$

When $k = -1$ (a thin pendent rivulet), (2.13) admits the family of solutions (Wilson & Duffy, 2005)

$$\zeta(y) = \frac{1}{2}h_{\mathrm{m}}\left[1 - (-1)^n\cos(y)\right] \tag{2.14}$$

defined only for $a = n\pi$ ($n \in \mathbb{N}$) but for any value of $h_{\mathrm{m}} > 0$. Such a solution represents n identical adjacent rivulets, each of maximum thickness h_{m}; the total half-area A of the solution is given by $A = \frac{1}{2}h_{\mathrm{m}}n\pi$. Thus in the lubrication limit, for a given solution branch indexed by n the half-width a is independent of A but the maximum thickness h_{m} may be chosen freely to satisfy a given choice of A.

As we will see, these solutions fail to capture the behaviour of the system for rivulets of non-vanishing thickness.

When $0 < \beta < \pi/2$, the lubrication solution satisfying (2.11) becomes

$$\zeta(y) = \frac{\tan(\beta)}{\sin(a)}\left(\cos(y) - \cos(a)\right), \tag{2.15}$$

with a single free parameter a. We shall return to this in Section 5.

REMARK 2. When $k = 1$ (a thin sessile rivulet), (2.13) has no non-zero solution. The absence of a solution in the lubrication limit does reflect the behaviour of solutions to the full (non-lubrication) system; we discuss this briefly in Section 6.

2.2 *Alternative approach using arclength*

Our approach to the problem will involve 'splicing together' two phase planes, corresponding to $k = \pm 1$. An alternative formulation (e.g. Liu *et al.*, 2014; Roman *et al.*, 2020) employs arclength along the free surface as the independent variable and an angle representing the free-surface slope as the dependent variable. In these variables the dynamics can be seen to be equivalent to those of a non-linear pendulum, where a single phase plane contains most of the required information.

Although the problem is reducible to a simple Hamiltonian system (see e.g. Eq. (10) in Liu *et al.* (2014)), we are not aware of analytic results such as we present here using the tools of time maps as in Burns & Grinfeld (2011). Usually, as in Liu *et al.* (2014) the Hamiltonian system is solved implicitly using elliptic integrals that have to be evaluated numerically or the non-linear pendulum equations are solved numerically. Although the time-map theorems we prove in this paper can in principle be proved in the non-linear pendulum framework, some extra manipulation is typically required to achieve this and in previous work time maps have had to be evaluated numerically (see e.g. Costa *et al.* (2021) for such an analysis). Therefore, although the arclength-based approach with a single phase plane complements this work, we use $\zeta(y)$ for analytical convenience.

3. Phase planes and construction of solutions

3.1 *Phase planes*

We define

$$p(y) = \zeta'(y) \qquad \text{and} \qquad q(y) = \frac{p'}{k(1+p^2)^{3/2}}, \tag{3.1}$$

so that (2.10) becomes the system

$$\begin{cases} p' = k(1+p^2)^{3/2} q, \\ q' = p. \end{cases} \tag{3.2}$$

It will be helpful when interpreting the solutions to note that while $p(y)$ describes the local gradient of the free surface, $q(y)$ represents both the pressure within the rivulet and (to within an additive constant) the profile $\zeta(y)$.

The contact-line conditions (2.12b) become

$$p(\pm a) = 0. \tag{3.3}$$

We will see later how to deal with the conditions $\zeta(\pm a) = 0$ [equation (2.12a)].

At a critical point $y = y_0$, two sections of the free surface $z = \zeta_1$ and $z = \zeta_2$ meet; the values of k on these two sections must be different. In the obvious notation, we must have

$$\begin{cases} p_1 \to \pm\infty \quad \text{and} \quad p_2 \to \mp\infty, \\ q_1 \to q_\infty \quad \text{and} \quad q_2 \to q_\infty \end{cases} \tag{3.4}$$

for some finite value q_∞, as $y \to y_0$. (The condition on q is obtained from (2.3), noting the change in sign due to the different values of k on the two sections of the free surface.)

The system (3.2) has a conserved quantity

$$H(p, q; k) = 1 + \frac{k}{(1 + p^2)^{1/2}} + \frac{1}{2}q^2, \tag{3.5}$$

to which we shall refer informally as the energy of a solution (although it does not represent a physical energy). An orbit in the (p, q) phase plane corresponding to $k = \pm 1$ therefore corresponds to a contour $H(p, q; \pm 1) = E_\pm$; this will be crucial to the construction.

Figure 2(a) illustrates the phase plane for $k = -1$. Closed orbits (blue in the figure) correspond to $0 < E_- < 1$; such orbits intersect the q-axis at $q = \pm q_0(E_-)$ and intersect the p-axis at $p = \pm p_0(E_-)$, where

$$q_0(E) = \sqrt{2E} \qquad \text{and} \qquad p_0(E) = \frac{\sqrt{2E - E^2}}{1 - E}. \tag{3.6}$$

Similarly, unbounded orbits (grey in the figure) correspond to $E_- > 1$; these intersect the q-axis at $q = \pm q_0(E_-)$ and satisfy $|q| \to q_\infty(E_-)$ as $|p| \to \infty$, where

$$q_\infty(E) = \sqrt{2(E - 1)}. \tag{3.7}$$

The critical orbit corresponding to $E_- = 1$ is shown in red. We will discuss the significance of the orbit corresponding to $E_- = E^*$ (shown in dashed red) in Section 3.4.

Figure 2(b) illustrates the phase plane for $k = +1$. Orbits that are bounded in p (blue in the figure) correspond to $1 < E_+ < 2$; such orbits intersect the p-axis at $p = \pm p_0(E_+)$. Similarly, orbits that are unbounded in p (grey in the figure) correspond to $E_+ > 2$; these intersect the q-axis at $q = \pm q_0(E_+)$. All orbits satisfy $|q| \to q_\infty(E_+)$ as $|p| \to \infty$. The separatrix corresponding to $E_+ = 0$ is shown in black. We will discuss the significance of the orbit corresponding to $E_+ = E^*$ (shown in dashed red) in Section 3.4.

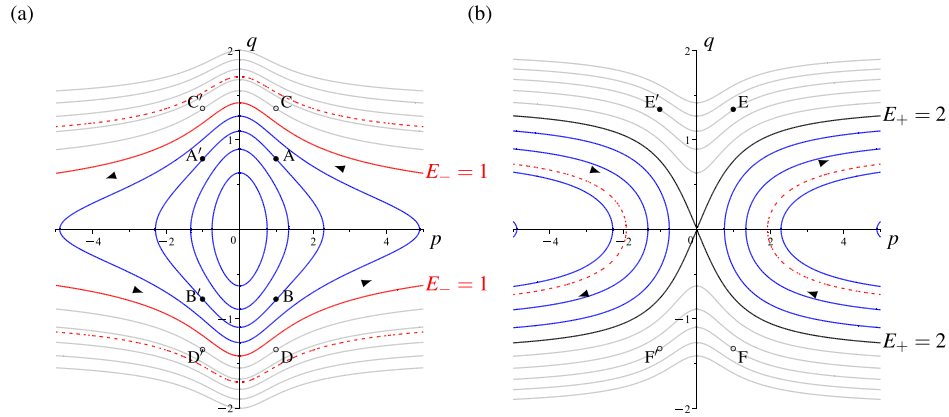

FIG. 2. Phase portraits of (3.2) with (a) $k = -1$ and (b) $k = +1$; orbits correspond to $H(p, q, ; \pm 1) = E_\pm$. In (a) closed orbits (blue) represent energies $0 < E_- < 1$; unbounded orbits (grey) represent energies $E_- > 1$; the solid red orbit represents $E_- = 1$. In (b) p-bounded orbits (blue) represent energies $1 < E_+ < 2$; $p-$unbounded orbits (grey) represent energies $E_+ > 2$; the separatrix (black) represents $E_+ = 2$. The dashed red orbit in each plot represents $E_+ = E^* \approx 1.462$ (see Section 3.4). The arrows indicate the direction of travel in each quadrant as y increases. Labels A through F′ are discussed in Section 5.

3.2 *Time maps*

We can rearrange the equation $H(p, q; k) = E$ to obtain

$$\frac{\mathrm{d}q}{\mathrm{d}y} = \pm \left[\frac{1}{(E - 1 - \frac{1}{2}q^2)^2} - 1 \right]^{1/2}. \tag{3.8}$$

The 'time' taken to traverse an orbit from $q = q_1$ to $q = q_2 > q_1$ (in physical terms, the lateral distance between these two points) is therefore given by

$$L(q_1, q_2; E) = \int_{q_1}^{q_2} \left[\frac{1}{(E - 1 - \frac{1}{2}q^2)^2} - 1 \right]^{-1/2} \mathrm{d}q = \int_{q_1}^{q_2} \frac{|2(E-1) - q^2|\,\mathrm{d}q}{\left[(2E - q^2)(4 - 2E + q^2)\right]^{1/2}}. \tag{3.9}$$

3.3 *Construction of pendent solutions with small energy*

We first consider the construction of solutions for pendent rivulets with small energy, for which the liquid lies above the air at every point on the free surface ($k = -1$). Such a solution corresponds to a closed orbit in the $k = -1$ phase plane, which we characterize by $H(p, q; -1) = E_-$, where $0 < E_- < 1$. As we have seen, the orbit intersects the q-axis at $q = \pm q_0(E_-)$ and the p-axis at $p = \pm p_0(E_-)$.

REMARK 3. Although we restrict ourselves here to solutions that traverse the orbit once, it is clear that we can construct solutions that traverse it any whole number of times, corresponding to $n \geq 2$ in the lubrication solution (2.14); for an illustration of such arrays of solutions, see fig. 4 of Sumesh & Govindarajan (2010). We also restrict ourselves to physically meaningful solutions $\zeta \geq 0$; each such solution has a counterpart unphysical solution $\zeta \leq 0$, which is constructed by starting at $q = +q_0(E_-)$.

The half-width of the rivulet is given from (3.9) by

$$a(E_-) = L(-q_0(E_-), q_0(E_-); E_-) = \int_{-\sqrt{2E_-}}^{\sqrt{2E_-}} \frac{2(1-E_-)+q^2}{\left[(2E_- - q^2)(4-2E_-+q^2)\right]^{1/2}}\mathrm{d}q. \tag{3.10}$$

Proposition 1. The half-width $a(E_-)$ given by (3.10) is a monotonically decreasing function of E_- on $0 < E_- \leq 1$.

Proof. See Appendix A.1. □

The maximum gradient occurs when $q = 0$, and is given by $p_0(E_-)$; as $E_- \to 1^-$, $p_0(E_-) \to \infty$. The critical orbit $E_- = 1$ thus corresponds to a rivulet profile which becomes vertical at $y = \pm\frac{1}{2}a(1)$. We may evaluate the half-width of this critical solution as

$$a(1) = \int_{-\sqrt{2}}^{\sqrt{2}} \frac{q^2}{\left[4-q^4\right]^{1/2}}\mathrm{d}q = 4E_I\left(\frac{1}{\sqrt{2}}\right) - 2K_I\left(\frac{1}{\sqrt{2}}\right) \approx 1.694, \tag{3.11}$$

where K_I and E_I are the complete elliptic integrals of the first and second kind.

Finally, we impose the boundary conditions $\zeta(\pm a) = 0$ by setting $\zeta(y) = q(y) + q_0(E_-)$. It follows that the maximum thickness of the rivulet is $h_\mathrm{m} = 2q_0(E_-) = 2\sqrt{2E_-}$. Further, the symmetry of the orbits in q means that we can easily calculate the half-area

$$A(E_-) = \int_{-a(E_-)}^{0} \zeta(y)\,\mathrm{d}y = \int_{-a(E_-)}^{0} \big(q(y) + q_0(E_-)\big)\,\mathrm{d}y = q_0(E_-)a(E_-). \tag{3.12}$$

Figure 3 illustrates a typical solution. The orbit in the phase plane is traversed anticlockwise from $(0, -q_0)$ and the profile is traversed from $y = -a$ to $y = +a$. Note that the symmetry of the orbit under reflection in the p- and q-axes corresponds to symmetry between the upper and lower parts, as well as the left- and right-hand parts, of the profile.

3.4 *Construction of pendent solutions with larger energy*

Orbits in the $k = -1$ phase plane corresponding to energies $E_- > 1$ do not connect two points on the q-axis and therefore cannot satisfy the boundary-value problem (3.2), (3.3). Instead, the argument of Section 2 leading to (2.2) shows that we must construct an 'overhanging' rivulet profile by connecting sections of the free surface on which liquid lies above air ($k = -1$) with sections on which liquid lies below air ($k = +1$). These sections must be connected at critical points at which the free surface becomes vertical and the conditions (2.3) (and thus (3.4)) apply.

We describe the construction of a rivulet with a single overhang between two critical points y_1 and y_2 with $y_1 < y_2$; we will show (Remark 4) that rivulets with multiple overhangs are impossible. The section of the free surface between the contact line $y = -a$ and the first critical point $y = y_2$ is given by $z = \zeta_1(y)$; on this section, liquid lies above air, $k = -1$. The section between the critical points $y = y_2$ and $y = y_1$ is given by $z = \zeta_2(y)$; on this section, liquid lies below air, $k = +1$. The section between the critical point $y = y_1$ and the midline of the rivulet $y = 0$ is given by $z = \zeta_3(y)$; on this section, liquid again lies above air, $k = -1$. (The reader may find it helpful to refer to Fig. 4). Once we have constructed the free surface between $y = -a$ and $y = 0$, the other half follows by symmetry.

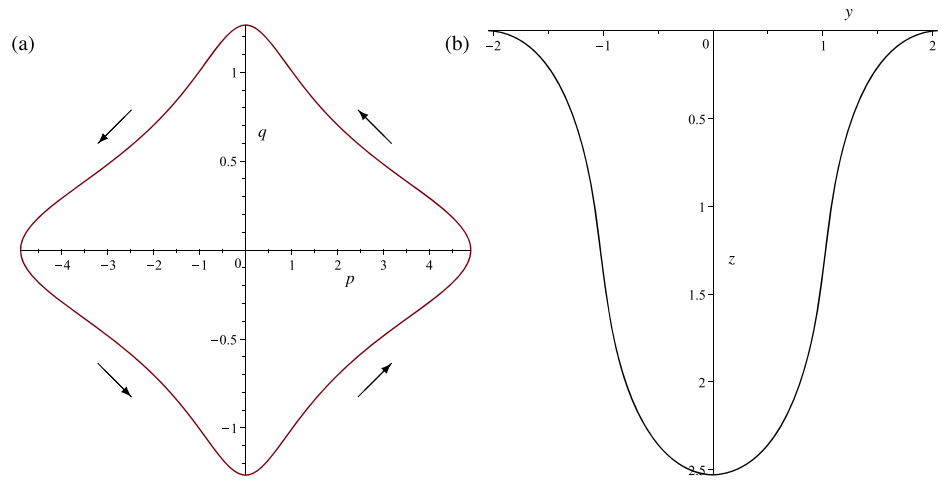

FIG. 3. The solution corresponding to $E_- = 0.8$. (a) The orbit in the (p, q) phase plane; arrows show y increasing. (b) The rivulet profile $z = \zeta(y)$ (note that the z-coordinate increases downwards). We have $q_0(E_-) \approx 1.265$, $a(E_-) \approx 2.042$, $A(E_-) \approx 2.584$.

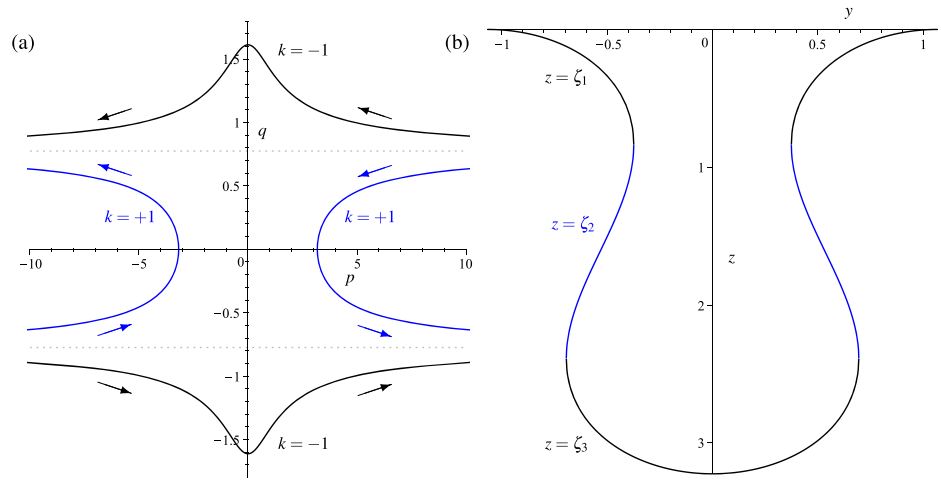

FIG. 4. The solution corresponding to $E = 1.3$. (a) The orbit in the (p, q) phase plane. (b) The rivulet profile made up of the sections $z = \zeta_1(y)$, $z = \zeta_2(y)$ and $z = \zeta_3(y)$ (note that the z-coordinate increases downwards). The sections and arrows in black correspond to the $k = -1$ phase plane; arrows show y increasing. The sections and arrows in blue correspond to the $k = +1$ phase plane; arrows show y decreasing. The dotted grey lines in (a) are $q = \pm q_\infty(E)$. We have $q_0(E) \approx 1.612$, $q_\infty(E) \approx 0.775$, $a(E) \approx 1.068$, $A(E) \approx 1.722$.

The construction proceeds as follows, for an energy $E_- > 1$.

(i) To construct $\zeta_1(y)$ between the contact line $y = -a$ and the critical point $y = y_2$, we start at $(p, q) = (0, -q_0(E_-))$ in the $k = -1$ phase plane, and follow this orbit in the direction of increasing y until $(p, q) \to (\infty, -q_\infty(E_-))$.

(ii) By (3.4), this orbit now connects to the orbit in the $k = +1$ phase plane, which satisfies $(p, q) \to (-\infty, -q_\infty(E_-))$. Setting $q_\infty(E_-) = q_\infty(E_+)$, we determine that the corresponding energy in the $k = +1$ phase plane is $E_+ = E_-$.

(iii) To construct $\zeta_2(y)$ between the critical points $y = y_2$ and $y = y_1$, we follow this orbit in the $k = +1$ phase plane in the direction of *decreasing* y from $(p, q) \to (-\infty, -q_\infty(E_+))$ to $(p, q) \to (-\infty, q_\infty(E_+))$.

(iv) By (3.4), this orbit now connects to the orbit in the $k = -1$ phase plane, which satisfies $(p, q) \to (\infty, q_\infty(E_-))$.

(v) To construct $\zeta_3(y)$ between the critical point $y = y_1$ and the midline $y = 0$, we follow this orbit in the $k = -1$ phase plane in the direction of increasing y from $(p, q) \to (\infty, q_\infty(E_+))$ to $(p, q) = (0, q_0(E_-))$.

(vi) The rest of the construction follows by symmetry.

Having shown that $E_- = E_+$ on any given solution, from this point onwards we omit the subscripts and write simply E.

To determine the critical points y_1 and y_2 and the half-width a we again use the 'time map' (3.9). From the construction described above, we have

$$y_2 - (-a) = L_-(E) = L(-q_0(E), -q_\infty(E); E), \tag{3.13}$$

$$y_2 - y_1 = L_+(E) = L(-q_\infty(E), q_\infty(E); E), \tag{3.14}$$

$$0 - y_1 = L(q_\infty(E), q_0(E); E) = L_-(E). \tag{3.15}$$

Thus

$$y_1 = -L_-(E), \qquad y_2 = -L_-(E) + L_+(E), \tag{3.16}$$

and

$$a(E) = 2L_-(E) - L_+(E). \tag{3.17}$$

PROPOSITION 2. The half-width $a(E)$ given by (3.17) is a monotonically decreasing function of E on $1 \le E < 2$.

Proof. See Appendix A.2. □

The half-area A is again straightforward to calculate, because the symmetry of the profile leads to many cancellations; it can readily be shown that it is given by

$$\begin{aligned} A(E) &= \int_{y_1}^{0} (\zeta_3 + q_0)\,\mathrm{d}y - \int_{y_1}^{y_2} (\zeta_2 + q_0)\,\mathrm{d}y + \int_{-a}^{y_2} (\zeta_1 + q_0)\,\mathrm{d}y \\ &= q_0(E)a(E) \end{aligned} \tag{3.18}$$

as for the low-energy solution. We will plot the half-area against the half-width in Section 4.

Figure 4 illustrates a typical solution. The orbit starts in the $k = -1$ phase plane at $(0, -q_0(E))$ and follows the construction described above. Note the symmetry of the profile within the middle section (blue in the figure) and between the upper and lower sections (black in the figure).

REMARK 4. It is clear from the construction described above that the solution must return to $(p, q) = (0, -q_0(E))$ after having fully traversed two unbounded orbits in the $k = -1$ phase plane and two in the $k = +1$ phase plane. This demonstrates that it is not possible to construct solutions that traverse the orbit once and have more than a single overhang; see also Remark 3.

3.5 *Pinch-off*

From Proposition 2 we see that as the energy E increases, the extent of the overhanging (blue) region increases and the overall width of the rivulet decreases. As a consequence, the profile eventually 'pinches off' when the first transition point occurs at $y = 0$; the self-intersection occurs at some $z = \zeta_p 0$. Pinch-off occurs when $E = E^* \in (1, 2)$ such that

$$L_-(E^*) = L_+(E^*). \tag{3.19}$$

PROPOSITION 3. The value of E^* is unique.

Proof. Since (from the proof of Proposition 2), $L_-(E^*)$ is monotonically decreasing in E^* and $L_+(E^*)$ is monotonically increasing in E^*, the value of E^* that satisfies (3.19) is unique. We may determine the value of E^* numerically as $E^* \approx 1.462$. □

For values of $E > E^*$, rivulet profiles can still be constructed as described in Section 3.4, but they are now self-intersecting and do not describe a physically realisable free surface. We can still define the half-area of a self-intersecting solution, and will do so when we construct bifurcation diagrams in Section 4. However, it is important to note that self-intersection is a topological change that is not captured when the bifurcation diagrams are plotted in terms of half-area.

PROPOSITION 4. For the pinch-off solution with $E = E^*$, the region enclosed by the free surface for $z > \zeta_p$ has half-area 1.

Proof. See Appendix A.3. □

4. Bifurcation analysis

Although we have used E as the control parameter when constructing solutions, it is convenient instead to regard the half-width a as the parameter; by Propositions 1 and 2 we know that a is a monotonically decreasing function of E. To characterize a solution we consider the half-area A; for $0 \leq E \leq 1$ this can be thought of as the L^1-norm of the solution $\zeta(y)$, while for $E > 1$ we may interpret it as the L^1-norm of a suitably defined (discontinuous) weak solution constructed using an equal-area rule. (For such a construction in an analogous problem, see Burns & Grinfeld (2011)).

Figure 5 shows the half-width A plotted against a for $0 \leq E \leq 1.7$. The following propositions establish the crucial features of this plot.

PROPOSITION 5. The non-trivial solution branch emerges from the trivial solution branch $\zeta \equiv 0$ through a pitchfork bifurcation at $(a, A) = (\pi, 0)$.

Proof. See Appendix A.4. □

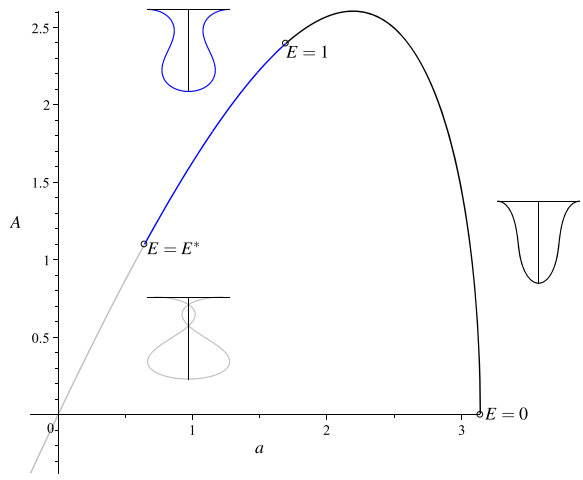

FIG. 5. The half-area A of a rivulet plotted against the half-width a. The black portion of the curve represents $0 < E < 1$ (rivulets without an overhang; the blue portion represents $1 < E < E^*$ (rivulets with an overhang); the grey portion represents $E > E^*$ (unphysical rivulets with a self-intersecting free surface). The insets (not to scale) indicate the form of the rivulet in each case.

PROPOSITION 6. The value of E at which the non-trivial solution branch passes through $(a, A) = (0, 0)$ satisfies $E > E^*$.

Proof. The solution branch passes through the origin when $a(E) = 0$ and thus $A(E) = \sqrt{2E}a(E) = 0$ [equation (3.18)]. From (3.17), $a(E) = 0$ when $2L_-(E) = L_+(E)$. But we know from the proof of Proposition 2 that $L_-(E)$ is monotonically decreasing and $L_+(E)$ is monotonically increasing, and from equation (3.19) we know that the energy E^* satisfies $L_-(E^*) = L_+(E^*)$. Thus $a(E) = 0 \implies E > E^*$. □

REMARK 5. Proposition 6 means that pinch-off occurs before this solution branch reaches the origin. Numerically, we find that $a(E) = 0$ for $E \approx 1.652$ (recall that $E^* \approx 1.462$).

REMARK 6. The lubrication approximation analysis (Section 2.1) fails to capture the pitchfork bifurcation at $(a, A) = (\pi, 0)$. This is not surprising, as it is clear from Fig. 2(a) that the lubrication approximation corresponds to linearizing about the centre $(0, 0)$ in the $k = -1$ phase plane. As can also be seen from fig. 7 of Roman *et al.* (2020), this situation is mathematically equivalent to linearizing a non-linear oscillator about a non-hyperbolic equilibrium: the linearized system (simple harmonic motion) cannot predict the relationship between amplitude and period and cannot capture the other features of the phase plane, such as the separatrix. Another classical example occurs when linearizing the Euler elastica around a bifurcation point (Brown, 2014).

5. Imperfect wetting

In this section we present illustrative solutions and bifurcation diagrams for imperfect wetting, when the contact angle $\beta > 0$. It is harder to obtain analytical results for this problem, because some of the relevant time maps are no longer monotonic in E (cf. Proposition 2). Nevertheless, all the behaviour of these imperfectly wetting solutions can be understood in terms of the perfectly wetting solutions.

Imperfectly wetting rivulets satisfy the problem (2.10), (2.11) with $\beta \neq 0$. We will first consider cases $0 < \beta < \pi/2$ (in fluid-dynamical terms, a hydrophilic substrate), and then $\beta > \pi/2$ (a hydrophobic substrate).

5.1 *Hydrophilic substrate* ($0 < \beta < \pi/2$)

5.1.1 *Construction of solutions.* When $0 < \beta < \pi/2$, each solution corresponds to a trajectory that starts and ends in the $k = -1$ phase plane. Each solution is characterized by an energy E and by the starting value of $p = p_\beta = \tan(\beta)$. It is readily seen from the phase plane (Fig. 2(a)) that for any value of E there are two possible solutions; it is convenient to consider $E \leq 1$ and $E > 1$ separately.

For $E \leq 1$ solutions either run from A: (p_β, q_β) to A′: $(-p_\beta, q_\beta)$, or from B: $(p_\beta, -q_\beta)$ to B′: $(-p_\beta, -q_\beta)$, where

$$q_\beta = \left(\frac{2(1 + (E-1)\sqrt{1+p_\beta^2})}{\sqrt{1+p_\beta^2}} \right)^{1/2}. \tag{5.1}$$

Examples of these points are plotted on Fig. 2(a), taking $E = 0.6$ for AA′ and BB′, and $E = 1.2$ for CC′ and DD′.

Remark 7. Solutions cannot run, e.g. from A to B′, because such solutions cannot satisfy the boundary conditions $\zeta(\pm a) = 0$.

For a given value of $p_\beta > 0$ there is a minimum attainable value of the energy, given by

$$E = E_{\min}(p_\beta) = 1 - \frac{1}{\sqrt{1+p_\beta^2}}. \tag{5.2}$$

When $E = E_{\min}(p_\beta)$, the points A and B (and likewise A′ and B′) are identical.

Solutions of the form AA′, BB′ and CC′ all correspond to trajectories that lie entirely in the $k = -1$ phase plane. To construct solutions of the form DD′ we must connect trajectories in the $k = -1$ plane with trajectories in the $k = +1$ plane as in Section 3.4. (We omit the details here for brevity, as they contain no new ideas).

Figure 6 illustrates the profiles for $E = 0.6$ (AA′ and BB′) and $E = 1.2$ (CC′ and DD′). The small-area solution in each case can be obtained by truncating the high-area solution at an appropriate horizontal level, and indeed each solution can be obtained by truncating the perfectly wetting solution for the same energy. (This construction is made more explicit in Perazzo & Gratton (2004)).

Because the shape of the solutions depends only on E and not on p_β, pinch-off occurs at the same energy $E = E^*$ as for the perfectly wetting solutions. However, pinch-off does not affect CC′ solutions as these do not have an overhang.

5.1.2 *Bifurcation structure.* Figures 7 shows the bifurcation diagram in the (a, A)-plane for $p_\beta = 0.1$.

For $p_\beta > 0$, $q = 0$ is no longer a solution to the boundary-value problem and the pitchfork bifurcation (Proposition 5) is replaced by a saddle-node bifurcation (Fig. 7). There are two solution branches, so for a given half-width a there are two solutions: a small-A solution and a large-A solution.

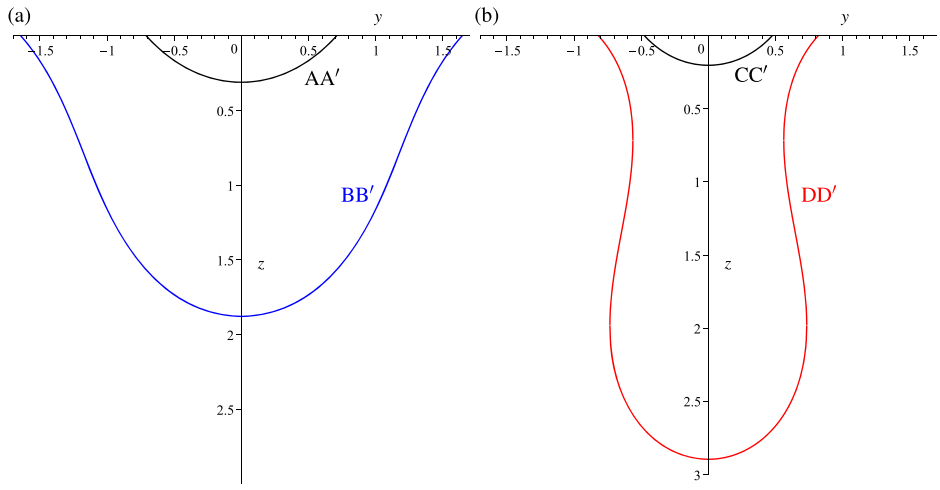

FIG. 6. The rivulet profiles $z = \zeta(y)$ for (a) $E = 0.6$ and (b) $E = 1.2$. In (a), the profile in black corresponds to the AA′ trajectory and the profile in blue corresponds to the BB′ trajectory. In (b), the profile in black corresponds to the CC′ trajectory and the profile in red corresponds to the DD′ trajectory. (See Fig. 2(a) in each case.)

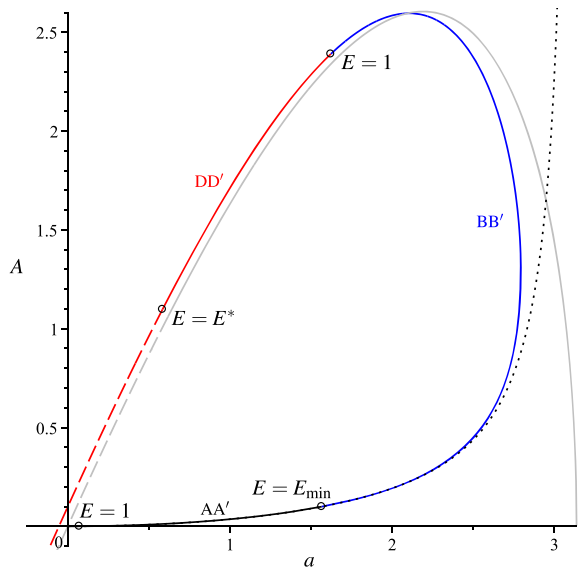

FIG. 7. The half-area A of a rivulet plotted against the half-width a, for $p_\beta = 0.1$. The black portion of the curve represents solutions of the form AA′ and CC′; the blue portion represents solutions of the form BB′; the red portion represents sections of the form DD′. The grey curve is for $p_\beta = 0$ (cf. Fig. 5). The dashed portions of each curve represent solutions beyond pinch-off. The dotted line is the asymptotic result (5.3) from lubrication theory.

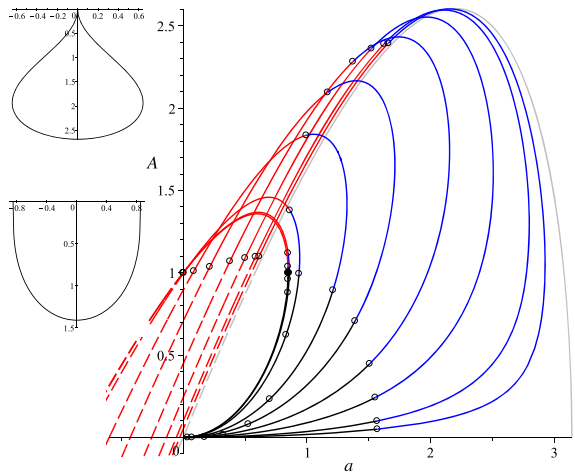

FIG. 8. The half-area A of a rivulet plotted against the half-width a, for $p_\beta = 0.05, 0.1, 0.25, 0.5, 1, 2, 10, 100$ and 1000. The black portion of each curve represents solutions of the form AA′ and CC′; the blue portion represents solutions of the form BB′; the red portion represents sections of the form DD′. The grey curve is for $p_\beta = 0$ (cf. Fig. 5). The dashed portions of each curve represent solutions beyond pinch-off. The open circles mark the points $E = 1$, $E = E_{\min}(p_\beta)$ and $E = E^*$ on each curve; the solid circle marks (a_∞, A_∞). The upper inset shows the profile of the rivulet in the limit $E = E^*$, $p_\beta \to \infty$; the lower inset shows the profile of the rivulet in the limit $E = 1$, $p_\beta \to \infty$.

REMARK 8. The lubrication approximation is premised on $|p| \ll 1$ (see Section 2.1), i.e. lubrication solutions are approximations to AA′ and CC′ solutions in the vicinity of the positive q-axis. Hence lubrication theory describes only the small-A solution branch.

From the solution (2.15) in the lubrication limit we obtain the asymptotic result

$$A(a) = p_\beta \left(1 - a\cot(a)\right), \tag{5.3}$$

which is plotted as a dotted line in Fig. 7. The asymptotic approximation (5.3) is usually described (cf. Wilson & Duffy, 2005) as valid for $p_\beta \ll 1$; however, as Fig. 7 illustrates, it is not uniformly valid in a because of the change in the bifurcation structure when $p_\beta > 0$.

Figure 8 illustrates further how the bifurcation diagram in the (a, A)-plane changes as p_β increases.

The limiting 'pinch-off' solution ($E = E^*$) in the limit as $p_\beta \to \infty$ is shown in the upper inset in Fig. 8. Pinch-off occurs for $\zeta_{\rm p} = 0$, giving a contact angle of $\pi/2$; this solution therefore has $a = 0$ by construction, and by Proposition 4 its half-area is $A = 1$.

In the limit as $p_\beta \to \infty$, $E_{\min}(p_\beta) \to 1$, and so the section of the curve corresponding to BB′ solutions disappears. The limiting solution without overhang (the lower inset in Fig. 8) corresponds to $E = 1$ and $p_\beta \to \infty$; its half-width is thus given by

$$a_\infty = \int_0^{\sqrt{2}} \frac{q^2}{[(2-q^2)(2+q^2)]^{1/2}} \mathrm{d}q = 2E_I\left(\frac{1}{\sqrt{2}}\right) - K_I\left(\frac{1}{\sqrt{2}}\right) \approx 0.847, \tag{5.4}$$

where E_I and K_I are elliptic integrals as before. The half-area of this limiting solution is given, using (3.8), by

$$A_\infty = \int_0^{\sqrt{2}} q \frac{\mathrm{d}y}{\mathrm{d}q} \mathrm{d}q = \int_0^{\sqrt{2}} \frac{q}{\left[4q^{-4} - 1\right]^{1/2}} \mathrm{d}q = 1. \tag{5.5}$$

5.2 *Hydrophobic substrate ($\beta > \pi/2$)*

When $\beta > \pi/2$, each solution corresponds to a trajectory that starts and ends in the $k = +1$ plane and is connected via the $k = -1$ plane. (In fact, every such solution corresponds to part of a DD′ solution as described above.) We omit the details of the construction as they can readily be deduced from Section 3.4, and give only a brief account of the results.

For given admissible values of E and $p_\beta < 0$, we define

$$q_\beta = \sqrt{2\left(E - 1 - \frac{1}{(1 + p_\beta^2)^{1/2}}\right)}. \tag{5.6}$$

Solutions either run from E to E′ or from F to F′, where E: (p_β, q_β), E′: $(-p_\beta, q_\beta)$, F: $(p_\beta, -q_\beta)$, F′: $(-p_\beta, -q_\beta)$, all in the $k = +1$ phase plane. Examples of these points are plotted on Fig. 2(b), taking $E = 2.6$ in each case.

For a given value of p_β, the energy E of an EE′ or FF′ solution must satisfy

$$E > E_\beta = 1 + \frac{1}{(1 + p_\beta^2)^{1/2}}. \tag{5.7}$$

Figure 9(a) shows the bifurcation diagram in the (a, A)-plane, and typical rivulet profiles, for a hydrophobic rivulet with $p_\beta = -2$. The EE′ branch (black) consists of physically valid solutions for all $E \geq E_\beta$; as $E \to \infty$, $(a, A) \to (0, 0)$. The FF′ branch (blue) consists of physically valid solutions for $E_\beta \leq E \lesssim 1.525$, at which point the half-width $a = 0$; for values of $E \gtrsim 1.525$, the solutions self-intersect (cf. fig. 3 of Sokurov, 2020). The value of E beyond which the solutions self-intersect depends on p_β, but must always be greater than E^*.

Figure 9(b) illustrates how the bifurcation diagram in the (a, A)-plane changes as p_β changes. As $p_\beta \to -\infty$, the contact angle $\beta \to \pi/2$ and so the curves approach the same limit as those for the hydrophilic problem in the limit $p_\beta \to \infty$ (see Fig. 8). As $|p_\beta|$ becomes smaller, the range of physically valid solutions decreases; for sufficiently small $|p_\beta|$, only solutions of the form EE′ are valid.

6. Discussion

We have presented an approach, based on phase-plane methods, to the problem of describing the free surface of a pendent rivulet. Although this problem has previously been tackled by other methods (e.g. Tanasijczuk *et al.*, 2010), the present approach allows us to make greater analytical progress, and in particular to carry out a more thorough bifurcation analysis.

In particular, our approach elucidates why lubrication theory fails to capture the behaviour of perfectly wetting pendent rivulets: the lubrication approach corresponds to linearizing around a centre

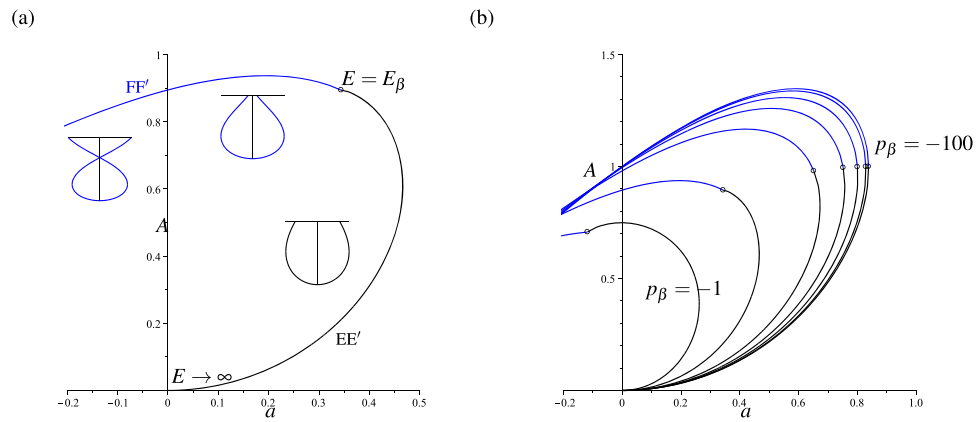

FIG. 9. (a) The half-area A of a rivulet plotted against the half-width a, for $p_\beta = -2$. The black portion of the curve represents solutions of the form EE′; the blue portion represents solutions of the form FF′. The insets (not to scale) indicate the form of the rivulet in each case. (b) The half-area A of a rivulet plotted against the half-width a, for $p_\beta = -1, -2, -5, -10, -20, -50$ and -100. The black portion of each curve represents solutions of the form EE′; the blue portion represents solutions of the form FF′. The open circles mark the point $E = E_\beta$ on each curve.

in the phase plane. This is analogous to linearizing a non-linear oscillator about a non-hyperbolic equilibrium; another classical example occurs when linearizing the Euler elastica around a bifurcation point (Brown, 2014). For imperfectly wetting pendent rivulets, lubrication theory provides a good approximation to one of the two solution branches when the rivulet is narrow, but the asymptotic approximation even to this branch is not uniform in the half-width a.

A feature of our approach, which appears to be novel, is that we 'splice together' solutions from orbits in two related phase planes. We suggest that this could be a useful technique in other problems that can be formulated such that the governing equation changes discontinuously but the solution itself does not. As an example, consider the problem of horizontal or vertical liquid bridges treated e.g. by Haynes *et al.* (2016) using the arclength formulation. These authors had to assume smallness of the Bond number and resort to asymptotics. We believe that our method could be useful in settling analytically the various mathematical questions raised by that paper, e.g. the relation between the upper and lower angles of the bridge.

Finally, we note that our approach can readily be applied to the corresponding problem for sessile rivulets. For sessile rivulets on hydrophilic surfaces, $0 < \beta < \pi/2$, solutions correspond to orbits in the $k = +1$ phase plane. Because the origin in this phase plane is a saddle point, linearizing about it correctly captures the behaviour (Perazzo & Gratton, 2004): in particular, lubrication theory correctly predicts (Wilson & Duffy, 2005) that there are no solutions for perfectly wetting sessile rivulets. For sessile rivulets on hydrophobic surfaces, $\beta > \pi/2$, solutions correspond to orbits that start and end in the $k = -1$ phase plane and are connected via the $k = +1$ phase plane; they may be constructed analogously to those described in Section 5.2.

Acknowledgments

We are grateful to Brian R. Duffy and Stephen K. Wilson for discussions of the rivulet problem over the course of several years, and to the anonymous reviewers for their insightful and constructive comments on two earlier versions of this manuscript.

Data availability

The mathematical content of the manuscript is selfcontained.

References

Batchelor, G. K. (1967) *An Introduction to Fluid Dynamics*. Cambridge University Press, Cambridge.

Brown, R. F. (2014) *A Topological Introduction to Nonlinear Analysis*. Heidelberg: Birkhäuser.

Burns, M. & Grinfeld, M. (2011) Steady state solutions of a bi-stable quasi-linear equation with saturating flux. *Eur. J. Appl. Math.*, **22**, 317–331.

da Costa, F. P., Grinfeld, M., Mottram, N. J., Pinto, J. T. & Xayxanadasy, K. (2021) Steady state solutions in a model of a cholesteric liquid crystal sample. *Afrika Mat. (3)*, **32**, 645–672.

Duffy, B. R. & Moffatt, H. K. (1995) Flow of a viscous trickle on a slowly varying incline. *Chem. Eng. J.*, **60**, 141–146.

Golubitsky, M. & Schaeffer, D. G. (1985) *Singularities and Groups in Bifurcation Theory*. New York: Springer-Verlag.

Haynes, M., O'Brien, S. B. G. & Benilov, E. S. (2016) Asymptotics of a horizontal liquid bridge. *Phys. Fluids*, **28**, 042107.

Liu, J., Sun, J. & Liu, L. (2014) Elastica of a pendant drop: Analytical solution in two dimension. *Int. J. Nonlinear Mech.*, **58**, 184–190.

Majumdar, S. R. & Michael, D. H. (1976) The equilibrium and stability of two dimensional pendent drops. *Proc. R. Soc. London A*, **351**, 89–115.

Neumann, F. (1894) *Die Theorie der Capillarität*. Leipzig: B. G. Teubner.

Paterson, C., Wilson, S. K. & Duffy, B. R. (2013) Pinning, de-pinning and re-pinning of a slowly varying rivulet. *Eur. J. Mech. B / Fluids*, **41**, 94–108.

Paterson, C., Wilson, S. K. & Duffy, B. R. (2014) Rivulet flow round a horizontal cylinder subject to a uniform shear stress. *Q. J. Mech. Appl. Math.*, **67**, 567–597.

Perazzo, C. A. & Gratton, J. (2004) NavierStokes solutions for parallel flow in rivulets on an inclined plane. *J. Fluid Mech.*, **507**, 367–379.

Pitts, E. (1973) The stability of pendent liquid drops, part 1. Drops formed in a narrow gap. *J. Fluid Mech.*, **59**, 753–767.

Roman, B., Gay, C. & Clanet, C. (2020) Pendulums, drops and rods: A physical analogy arXiv preprint arXiv:2006.02742.

Schaaf, R. (1991) *Global solution branches of two point boundary value problems*. *Number 1458 in Lecture Notes in Mathematics*. Springer-Verlag, Berlin Heidelberg.

Snoeijer, J. H. (2006) Free-surface flows with large slopes: Beyond lubrication theory. *Phys. Fluids*, **18**, 021701–021701.

Sokurov, A. A. (2020) Exact solutions of the shaping problem in two-dimensional case and their properties. *Vestnik BGU, Ser 1. Fizika. Mat.*, **(4)**, 99–111.

Sullivan, J. M., Wilson, S. K. & Duffy, B. R. (2008) A thin rivulet of perfectly wetting fluid subject to a longitudinal surface shear stress. *Q. J. Mech. Appl. Math.*, **61**, 25–61.

Sumesh, P. T. & Govindarajan, R. (2010) The possible equilibrium shapes of static pendant drops. *J. Chem. Phys.*, **133**, 144707.

Tanasijczuk, A. J., Perazzo, C. A. & Gratton, J. (2010) Navier–stokes solutions for steady parallel-sided pendent rivulets. *Eur. J. Mech. B / Fluids*, **29**, 465–471.

Wilson, S. K. & Duffy, B. R. (2005) A rivulet of perfectly wetting fluid draining steadily down a slowly varying substrate. *IMA J. Appl. Math.*, **70**, 293–322.

A. Proofs

A.1 *Proof of Proposition 1*

Proof. By the change of variables $q^2 = 2E_- u$ we can write

$$a(E_-) = \sqrt{2}\int_0^1 \frac{1-(1-u)E_-}{[u(1-u)(2-(1-u)E_-)]^{1/2}}\mathrm{d}u. \tag{A.1}$$

It follows that

$$\frac{\mathrm{d}}{\mathrm{d}E_-}a(E_-) = \frac{1}{\sqrt{2}}\int_0^1 \frac{-(1-u)^{1/2}(3-(1-u)E_-)}{[u(2-(1-u)E_-)^3]^{1/2}}\mathrm{d}u. \tag{A.2}$$

Since $0 < E_- \leq 1$, the integrand is negative and thus $a(E_-)$ given by (3.10) is monotonically decreasing as required. □

A.2 *Proof of Proposition 2*

Proof. We first show that $L_-(E)$ is a monotonically decreasing function of E. By the change of variables $q^2 = 2Eu$, we can write

$$L_-(E) = \frac{1}{\sqrt{2}}\int_{1-1/E}^1 \frac{1-(1-u)E}{[u(1-u)(2-(1-u)E)]^{1/2}}\mathrm{d}u. \tag{A.3}$$

It follows after a little algebraic manipulation that

$$\frac{\mathrm{d}L_-}{\mathrm{d}E} = \frac{1}{2\sqrt{2}}\int_{1-1/E}^1 \frac{-(3-(1-u)E)(1-u)}{[u(1-u)(2-(1-u)E)]^{1/2}(2-(1-u)E)}\mathrm{d}u. \tag{A.4}$$

Since $1 \leq E < 2$ and $0 < u \leq 1$, the integrand is negative and thus $L_-(E)$ is monotonically decreasing in E as required.

We now show that $L_+(E)$ is a monotonically increasing function of E. By the change of variables $q^2 = 2(E-1)u$, we can write

$$L_+(E) = 2(E-1)^{3/2}\int_0^1 \frac{1-u}{[u(E-(E-1)u)(2-E+(E-1)u)]^{1/2}}\mathrm{d}u. \tag{A.5}$$

Now, $(E-1)^{3/2}$ is a monotonically increasing function of E, and it follows after a little more algebraic manipulation that

$$\frac{\mathrm{d}}{\mathrm{d}E}\int_0^1 \frac{1-u}{[u(E-(E-1)u)(2-E+(E-1)u)]^{1/2}}\mathrm{d}u = \int_0^1 \frac{\sqrt{2}(E-1)(1-u)^3\mathrm{d}u}{[u(2-E+(E-1)u)(u+(1-u)E)]^{1/2}(E-(E-1)u)(2-E+(E-1)u)}. \tag{A.6}$$

Since $1 \leq E < 2$ and $0 < u \leq 1$, the integrand is positive and thus $L_+(E)$ is monotonically increasing in E as required.

It follows that the half-width $a(E)$ given by (3.17) is a monotonically decreasing function of E as required. □

A.3 *Proof of Proposition 4*

Proof. By construction, the half-area of the region concerned is given by

$$A_{\mathrm{p}} = \int_{-a}^{0} \zeta_3(y)\,\mathrm{d}y - \int_{-a}^{0} \zeta_2(y)\,\mathrm{d}y. \tag{A.7}$$

Using (3.8), we can rewrite this as

$$\begin{aligned} A_{\mathrm{p}} &= \int_{q_\infty(E^*)}^{q_0(E^*)} \frac{q\,\mathrm{d}q}{\left[\frac{1}{(1-E^*+\frac{1}{2}q^2)^2}-1\right]^{1/2}} + \int_{-q_\infty(E^*)}^{q_\infty(E^*)} \frac{q\,\mathrm{d}q}{\left[\frac{1}{(1-E^*+\frac{1}{2}q^2)^2}-1\right]^{1/2}} \\ &= \int_{-\sqrt{2(E^*-1)}}^{\sqrt{2E^*}} \frac{q\,\mathrm{d}q}{\left[\frac{1}{(1-E^*+\frac{1}{2}q^2)^2}-1\right]^{1/2}} = 1 \end{aligned} \tag{A.8}$$

by evaluating the integral directly. (We note that this result does not rely on the numerical value of E^*.) □

A.4 *Proof of Proposition 5*

Proof. The bifurcation point corresponds to $E = 0$. From (3.10) we have

$$a(E) = \int_{-\sqrt{2E}}^{\sqrt{2E}} \frac{2(1-E)+q^2}{\left[(2E-q^2)(4-2E+q^2)\right]^{1/2}}\mathrm{d}q = \sqrt{2}\int_{-1}^{1} \frac{1+(u^2-1)E}{[(1-u^2)(2+(u^2-1)E]^{1/2}}\,\mathrm{d}u, \tag{A.9}$$

and thus

$$\lim_{E\to 0} a(E) = \int_{-1}^{1} \frac{\mathrm{d}u}{\sqrt{1-u^2}} = \pi. \tag{A.10}$$

From (3.12) it follows that $A(E) = a(E)\sqrt{2E} \to 0$ as $E \to 0$. Thus the bifurcation point is $(a, A) = (\pi, 0)$ as required.

We recall from Remark 3 that every physical solution with $\zeta \geq 0$ and $A > 0$ has a counterpart unphysical solution with $\zeta \leq 0$ and thus $A < 0$. Further, we can expand the integrand in (A.9) to obtain

$$a(E) = \pi - \frac{3}{8}\pi E + o(E) \quad \text{and thus} \quad A(E) = \pi\sqrt{2E} + o(\sqrt{E}), \tag{A.11}$$

and thus

$$A(E) \sim \frac{4\sqrt{\pi}}{\sqrt{3}}(\pi - a)^{1/2} \tag{A.12}$$

on the physical branch of solutions $A > 0$.

From the symmetry of the solutions $A \gtrless 0$ and this local structure, it follows that the bifurcation at $a = \pi$ is a pitchfork. Non-trivial solutions exist for $a < \pi$. (This result can alternatively be obtained via Liapunov–Schmidt reduction (Golubitsky & Schaeffer, 1985)). □